L. HACKERMÜLLER
K. HORNBERGER
B. BREZGER[*]
A. ZEILINGER
M. ARNDT[✉]

Decoherence in a Talbot–Lau interferometer: the influence of molecular scattering

Institut für Experimentalphysik der Universität Wien, Boltzmanngasse 5, 1090 Wien, Austria

ABSTRACT This work describes the interference of C_{70} fullerenes in a Talbot–Lau interferometer with a large separation between the diffraction gratings. This permits the observation of recurrences of the interference contrast both as a function of the de Broglie wavelength and in dependence of the interaction of background gases. An exponential decrease of the fringe visibility with increasing background pressure was observed and good quantitative agreement with the predictions of decoherence theory was found. From extrapolation of the limits of matter wave interferometry it can be concluded that the influence of collisional decoherence may be well under control in future experiments with proteins and even larger objects.

PACS 03.75.-b; 03.65.Yz; 39.20.+q

1 Introduction

Matter wave interferometry of small quantum objects has become an active field of research during the last decades [1]. The new field of coherent optics with large molecules is now exploring the technical and possibly fundamental limits of interferometry with quantum objects of high mass, high internal complexity and high internal excitation – i.e. with novel properties which allows detailed study of the quantum-classical transition [2, 3].

Several challenges arise when one moves from small to large systems: At a given velocity the de Broglie wavelength $\lambda = h/(mv)$ shrinks with increasing mass, and in addition it becomes increasingly difficult to slow down massive systems which have a large kinetic energy. The requirements on interferometer technology for de Broglie wavelengths in the sub-picometer range are already rather demanding. But even more important are the potential mechanisms which may lead to decoherence, this is a loss of visibility in the interference pattern due to the coupling of the quantum system to its environment (see e.g. [4, 5]).

The investigation of this apparent loss of quantum properties has become an important corner stone of modern quantum physics – not only due to its fundamental role in mesoscopic physics and its importance for the understanding of the quantum-classical transition, but also because of its potential impact on emerging quantum technologies, such as quantum computers.

Any increase in size and complexity generally opens new decoherence channels, and for large molecules one can think of many interactions with the environment, either by scattered radiation [6], by collisions with particles [7], by an interaction with fluctuating quasi-static electro-magnetic fields [8], or even by the interaction with gravitational waves [9].

While it is impossible to manipulate and track the details of the perturbations for really macroscopic systems, the environment of isolated mesoscopic quantum systems can still be efficiently controlled. In the present paper focus is on one particular interaction between large molecules and an environment, namely collisions between the coherently propagating molecules and various background gases. First results on this subject have already been discussed in a previous letter [7]. In the present work more detailed background information is given on the quantitative investigations of collisional decoherence of the fullerene C_{70}, and also both experimental and theoretical studies of the influence of increased interaction times, which will be unavoidable in interferometry with proteins.

2 The Talbot–Lau interferometer

One can conceive various experimental arrangements to demonstrate the wave-nature of material particles and many interferometers have already been built for atoms (see refs. in [1]). Also for small molecules a number of arrangements such as grating diffraction [2, 11], Ramsey–Bordé interferometry [12, 13], or Mach–Zehnder interferometry [6, 14] have been shown to work. However, all these arrangements need well collimated beams or experimentally distinguishable internal states in order to separate the various diffraction orders. This requirement makes them less suitable for large clusters and large molecules for which brilliant sources and highly efficient detection schemes still have to be developed.

A near-field interferometer of the Talbot–Lau type, in contrast, does away with the collimation requirement. Unlike the

✉ Fax: +43-1/4277-9512, E-mail: markus.arndt@univie.ac.at
[*]*Present address*: Fachbereich Physik, Universität Konstanz, 78457 Konstanz, Germany

far-field interferometers, it is more compact, rugged and allows a much higher transmission [15].

The basic idea of such a device, the lens-less periodic imaging of molecular density distributions, can already be seen from a short discussion of the Talbot effect as used in light optics [16]. Suppose that a plane wave $\psi_0 = \exp(\mathrm{i}kz)$ illuminates a grating located in the (x, y)-plane with grating function $t(x)$. The wave function at a distance L behind the grating is then given in paraxial approximation by the Kirchhoff–Fresnel integral

$$\psi_L = \mathrm{e}^{\mathrm{i}kL} \left(\frac{k}{2\pi \mathrm{i} L} \right)^{\frac{1}{2}} \int \mathrm{d}x' t(x') \exp \left(\mathrm{i}k \frac{(x-x')^2}{2L} \right) .$$

It is easily evaluated if the grating function is periodic,

$$t(x) = \sum_{\ell \in \mathbb{Z}} a_\ell \exp \left(2\pi \mathrm{i} \ell \frac{x}{d} \right) , \tag{1}$$

and one finds by Gaussian integration,

$$\psi_L = \mathrm{e}^{\mathrm{i}kL} \sum_\ell a_\ell \exp \left(2\pi \mathrm{i} \ell \frac{x}{d} \right) \exp \left(-\mathrm{i}\pi \ell^2 \frac{L\lambda}{d^2} \right) .$$

From this expression one observes immediately that at even multiples of the distance

$$L_\lambda = \frac{d^2}{\lambda}$$

the transverse part of the wave function is simply given by the grating function (1). The grating pattern is also repeated at odd multiples of the *Talbot length* L_λ, but there it is shifted along x by half a grating period $d/2$.

This lens-less Talbot imaging is a pure interference effect and was already successfully applied to material objects [17, 18]. However, in the version described so far it still requires a plane wave, i.e., a parallel input beam. The full intensity gain of the Talbot effect is only deployed when it is applied to uncollimated and therefore much more intense molecular beams [19, 20]. This is realized if the single diffraction grating is replaced by three gratings, which act from front to end as a multiplexing collimator, a diffraction grating and a detection mask (for details see [21]). Each point in the first grating then acts as the source of an interference pattern and, even though there is no coherence between different source points, the independent interference patterns originating from each of them overlap in a position-synchronized manner to form a pattern of high fringe visibility. One may also regard the first grating as a tool to impose some coherence on the uncollimated molecular beam. The finite width of each opening in the first grating induces lateral coherence at the second grating which is of the order of 2–3 grating periods.

The experimental setup is based on this idea, and a sketch of it is shown in Fig. 1. C_{70} molecules are sublimated at 900 K to form an effusive beam with molecular de Broglie wavelengths in the range from 2 pm to 5 pm. The beam is essentially uncollimated in the horizontal direction, but it is selected by three spatially separated height delimiters, namely the oven aperture (200 μm), a central height delimiter (alternatively 50 or 150 μm), and the detector laser beam with
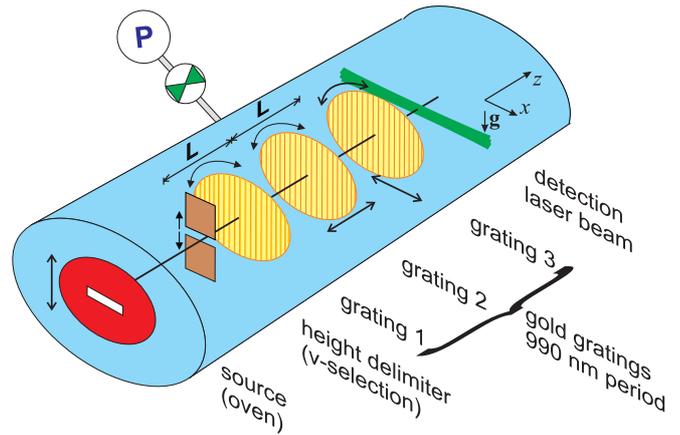

FIGURE 1 Artist's view of the 'pressurized' Talbot Lau interferometer. A beam of C_{70} molecules is generated from fullerene powder at 900 K. The beam passes a series of three gold gratings each with a grating constant of $d = 990$ nm, an open width of 480 nm and a grating thickness of 500 nm. The grating separation L was set to 38 cm. The whole vacuum chamber is evacuated to 2×10^{-8} mbar and can then be pressurized with different gases, typically up to 10^{-6} mbar. The fullerenes are detected using a laser induced thermal ionization process [10]. The interferogram is scanned by shifting the third grating along the grating vector

a waist of 10 μm. By shifting the oven vertically one can then select a well-determined free-flight parabola and thus a certain velocity class. This way, mean velocities could be chosen from 90 m/s to 220 m/s with the full width at a half maximum of their distributions ranging from 7% to 17% of the mean velocity. The gravitational method is superior to a set of rotating slotted disks because it avoids additional vibrations and allows up to 100% throughput at the central selected velocity.

The transverse coherence of the beam is unprepared until the molecules pass the first grating. The three gold gratings have a period of 990 nm, a nominal open fraction of 0.48 ± 0.02 (as specified by the manufacturer Heidenhain, Traunreut) and a flat open field of roughly 16 mm diameter. The lateral width of the molecular beam is of the order of 1 mm which is also comparable to the width of the ionization range of the detecting laser beam [10]. The distance between consecutive gratings was set to $L = 0.38$ m. This is almost twice as large as in previous experiments [7], and enables observation of two Talbot recurrences (see Fig. 2). All gratings can be rotated around the molecular beam to align them with an accuracy of about 1 mrad both with respect to each other and to the direction of earth's acceleration. The third grating G_3 masks the molecular density pattern behind the second grating. G_3 is mounted on a piezo translation stage (Piezosystem Jena) and is scanned perpendicular to the molecular beam in steps of 100 nm. The molecules which are in phase with the openings of G_3 pass the grating and are heated by the crossing Ar^+ laser beam (488 nm, 15 Watt). The positive ions which are generated by the laser induced thermionic emission are counted as a function of the lateral position x_s of G_3. As shown below, theory predicts an almost sine-wave shaped interferogram $S(x_s)$ for the transmitted molecules. This is indeed observed in the experiment, and the fringe contrast $V_\lambda = (S_{\max} - S_{\min})/(S_{\max} + S_{\min})$ serves to characterize the interference pattern.

The quantum origin of the observed signal is confirmed by the characteristic dependence of its contrast V_λ on the mo-
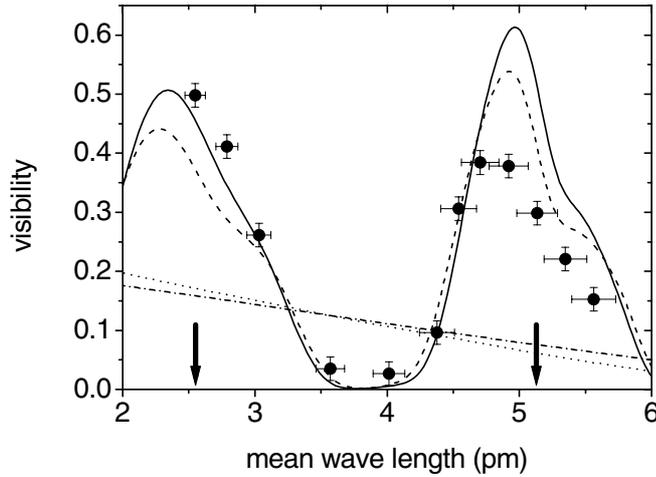
FIGURE 2 Interferometer visibility as a function of the mean molecular de Broglie wavelength. A clear recurrence of the interference maximum is observed both in the experiment (*circles*) and in the numerical model (*lines*). This is expected for the Talbot effect with varying wavelength or varying Talbot distance respectively. The pressure in the chamber was below 3×10^{-8} mbar so that collisions are still negligible, and the central height limiter was set to 50 μm. The theoretical lines correspond to the quantum calculation at open fractions of $f = 0.45$ (*solid line*) and $f = 0.48$ (*dashed line*), while the corresponding classical expectation is shown by the *dotted* ($f = 0.45$) and *dash-dotted line* ($f = 0.48$). The *arrows* indicate the wavelengths where the Talbot criterion $L = mL_\lambda, = mg^2/\lambda$, $m \in \mathbb{N}$, is met with $m = 1$ for $\lambda = 2.58$ pm and $m = 2$ for $\lambda = 5.16$ pm. With respect to ideal gratings the true maxima are slightly shifted to smaller wavelengths and the two maxima have different heights. This is due to the interaction between the molecule and the wall

lecular wavelength. If there is a coherent evolution in the interferometer the expected fringe signal is easily calculated, using wave optics in paraxial approximation. Starting with an incoherent beam one finds, after a coherent passage from the first to the third grating [20],

$$S(x_s) \propto \sum_{m \in \mathbb{Z}} \left(B_m^{(0)*} \right)^2 B_{2m}^{(\lambda)} \exp \left(2\pi i m \frac{x_s}{d} \right) \tag{2}$$

The coefficients B_m are defined in terms of the Fourier components a_ℓ of the transmission function (1) of each of the three equal gratings,

$$B_m^{(\lambda)} = \sum_{\ell \in \mathbb{Z}} a_\ell a_{\ell-m}^* \exp \left(i\pi \frac{m^2 - 2\ell m}{2} \frac{L}{L_\lambda} \right), \tag{3}$$

and

$$B_m^{(0)} = \sum_{\ell \in \mathbb{Z}} a_\ell a_{\ell-m}^* . \tag{4}$$

The $B_m^{(\lambda)}$ describe the diffraction at the second grating, while the $B_m^{(0)}$ belonging to the first and third grating serve to mask the molecular density. The Fourier coefficients a_ℓ also include the effect of the attractive interaction between molecule and grating in eikonal approximation [20, 21]. The masking by G_1 and G_3 is essentially wavelength independent. But due to the finite flight time of the molecules through the grating slits the van der Waals force introduces a certain wavelength dependence also in the $B_m^{(0)}$.

Before taking the experimental signal as evidence for quantum interference one must note that a certain fringe contrast could also be explained by classical mechanics due to

a shadow effect. The classical expectation can be calculated by propagating the classical phase space density of an uncollimated particle stream through the interferometer subjected to the same forces and approximations as in the quantum case. For ideal gratings the resulting expression is given by (2) after simply replacing the $B_{2m}^{(\lambda)}$ by $B_{2m}^{(0)}$ [22]. In the presence of van der Waals interactions the deflection tends to be underestimated in the classical analog of the eikonal approximation, so that the classical calculation gives an upper limit for the classical visibility. Hence, whenever the experimental contrast is significantly greater than the classical value one has evidence that quantum interference took place.

An even stronger proof is the characteristic wavelength dependence of the fringe visibility. Varying the mean molecular velocity corresponds to changing the mean molecular de Broglie wavelength. This dependence is used to scan the Talbot length L_λ and to demonstrate the periodic wave nature of the molecular Talbot–Lau effect in Fig. 2.

The experimental data are shown as full circles and are generally well represented by the quantum theoretical calculation (solid line). Both clearly show the expected recurrence of the visibility with λ. The classical expectation (dash-dotted line) completely fails to reproduce the observed effects. Note that the visibility peaks are neither equally high nor symmetric around their maxima. Also, the peaks do not occur exactly at the Talbot length (indicated by arrows in Fig. 2). Instead the maxima are shifted to shorter wavelengths and the peaks have a broad shoulder towards the longer wavelengths. These deviations from the simple optical Talbot–Lau effect appearing in the experiment are reproduced in the quantum calculation after taking into account the retarded van der Waals interaction [23] between the polarizable molecules and the gold bars of the gratings. This interaction reduces the effective slit width. At fixed grating distance this corresponds to a shift of the maxima towards smaller wavelengths.

Figure 2 shows two theoretical predictions which represent the experimental data. The dashed line assumes a grating with an open fraction, i.e. a ratio of opening to grating constant, of 0.48 as originally specified when the gratings were purchased and mounted about two years ago. The solid line assumes and open fraction of 0.45. A possible explanation for the apparent shrinking of the openings might be a deposited layer of fullerenes which are also visible to the unaided eye, at least on the first grating. But also tiny mechanical grating deformations might be a reason.

A notable difference is observed between theory and observation in the peak height at a wavelength around 5 pm, corresponding to molecules with a mean velocity of around 100 m/s. This is evidence for the hypothesis that the experimental reduction of the interference contrast is mainly due to remaining vibrations of the setup with oscillation amplitudes of a few ten nanometers. Further investigations of this effect are currently under way.

3 Collisional decoherence: A quantum system interacting with the environment

A controlled source of decoherence can now be introduced by filling the vacuum chamber with various gases at

low pressure ($p = 0.05...2.5 \times 10^{-6}$mbar) at room temperature. Each collision between a fullerene molecule and a gas particle entangles their motional states. Hence, the effect of a single collision on the molecular center-of-mass state is obtained by tracing over the state of the scattered molecule. One can safely assume that the mass of the fullerene molecule is much greater than the mass m_g of the gas particle. It is then found that the density operator, $\varrho_0(\boldsymbol{r}, \boldsymbol{r}')$, describing the quantum state of the fullerene molecules in position representation, changes simply by a multiplicative factor,

$$\varrho(\boldsymbol{r}, \boldsymbol{r}') = \varrho_0(\boldsymbol{r}, \boldsymbol{r}')\, \eta(|\boldsymbol{r} - \boldsymbol{r}'|)\,. \tag{5}$$

This factor η may be called the decoherence function since it describes the effective loss of coherence in the fullerene state. For elastic scattering with an isotropic potential and the gas initially in a thermal state it reads [24]

$$\eta(\delta r) = \int\limits_0^\infty \mathrm{d}v_g\, \frac{g(v_g)}{\sigma(v_g)} \int \mathrm{d}\Omega\, \left| f\left(\cos(\theta)\right) \right|^2$$
$$\times\, \mathrm{sinc}\left(\sin\left(\frac{\theta}{2}\right) \frac{2m_g v_g \delta r}{\hbar} \right)\,. \tag{6}$$

This expression involves an integration over the thermal distribution $g(v_g)$ of the gas velocities and an integral over the scattering angle $\Omega = (\theta, \phi)$. In the argument of the sine function one finds the distance of the considered points times the momentum change in units of $\hbar$. Hence, the sinc function suppresses the integrand whenever the change in the state of the gas particle during a collision is able to resolve the distance δr. This leads to a reduction of the corresponding off-diagonal elements in (5) when the gas particle transmits (partial) position information about the molecule to the environment. For small distances the sinc approaches unity so that the angular integral yields the total scattering cross section $\sigma(v_g)$. Hence, for $\delta r \to 0$ the decoherence function approaches unity as required from the conservation of the trace in (5).

By formulating the molecular evolution through the interferometer in the Wigner representation one finds that the effect of collisional decoherence can be treated analytically [22]. It is completely described by a modification of the coefficients (3). To obtain the interference signal in the presence of a gas the $B_{2m}^{(\lambda)}$ in (2) must be replaced by

$$B_{2m}^{(\lambda)} \exp\left(-n\sigma_{\mathrm{eff}} \int\limits_0^{2L} \left[1 - \eta\left(m\frac{L - |z - L|}{L_\lambda} d \right) \right] \mathrm{d}z \right)\,. \tag{7}$$

Here $n\sigma_{\mathrm{eff}}$ is the number density of gas particles times the effective total cross section defined below in (8), describing the number of collisions per unit length. The integral in the exponent covers the various positions in the interferometer where a collision may occur. As discussed above we have $\eta(0) = 1$, and the function decreases to zero for increasing arguments. It follows that the $m = 0$ component, related to the mean flux through the interferometer, is not affected by decoherence. The other components of the interference signal are most sensitive to collisions occurring close to the

second grating, at $z = L$, where the path separation is greatest. Indeed, if the Talbot criterion is met, $L = \ell L_\lambda$, $\ell \in \mathbb{N}$, the distances entering the decoherence function are integer multiples of the grating period d. For the other z positions the sensitivity decreases according to the path separation and, as one expects, a collision event will not contribute to decoherence directly at the first or at the third grating, at $z = 0,\ 2L$.

One can show that the general formula (7) is equivalent[1] to the solution in paraxial approximation of the master equation for the decoherence of a massive particle by interacting with a gas [24, 25]. The present form (7) has the advantage that it separates the rate of the decoherence events, the factor $n\sigma_{\mathrm{eff}}$, from their effect described by the integrand in (7). This is particularly useful if the two processes should be treated with different degrees of accuracy, as is the case in the present experiment.

At the prevailing (room) temperature of the experiment each collision with a gas particle is so strong that it serves to localize the fullerene to the scale of a few nanometers, which is small compared to the typical path separation of 1 µm. Therefore one can safely approximate the integral in (7) by $2L$ if $m \neq 0$. On the other hand, the effective scattering cross section must be evaluated with care, since it must account for the longitudinal velocity $v_m \boldsymbol{e}_z$ of the fullerene and for the thermal distribution $\mu(\boldsymbol{v}_g)$ of the gas particle velocities. The general expression reads

$$\sigma_{\mathrm{eff}}(v_m) = \int \mu(\boldsymbol{v}_g)\sigma(|v_m\boldsymbol{e}_z - \boldsymbol{v}_g|)\frac{|v_m\boldsymbol{e}_z - \boldsymbol{v}_g|}{v_m}\, \mathrm{d}\boldsymbol{v}_g\,. \tag{8}$$

In the experiment the interaction potential is well described by the isotropic London dispersion force (van der Waals force between polarizable molecules). The corresponding potential $U(r) = -C_6/r^6$ has a single parameter C_6 that can be found in [7] for a number of gases. The cross section $\sigma(v)$ for a fixed relative velocity follows from a semiclassical calculation [26] and the remaining integration in (8) can be performed asymptotically. This gives

$$\sigma_{\mathrm{eff}}(v_m) = \frac{4\pi\, \Gamma(9/10)}{5\sin(\pi/5)} \left(\frac{3\pi C_6}{2\hbar}\right)^{2/5} \frac{\tilde{v}_g^{3/5}}{v_m}$$
$$\times \left\{ 1 + \frac{1}{5}\left(\frac{\tilde{v}_g}{v_m}\right)^2 + \mathcal{O}\left(\frac{\tilde{v}_g}{v_m}\right)^4 \right\} \tag{9}$$

with $\tilde{v}_g = (2k_B T/m_g)^{\frac{1}{2}}$ the most probable velocity in the gas.

This effective cross section exceeds the geometric one by two orders of magnitude at the velocities of the experiment ($v_m = 80...240$ m/s).

A further simplification comes from the fact that for the experimental setup the visibility of the interference signal (2) is essentially determined by the $m = 0$ and $m = \pm 1$ Fourier components only. The expected reduction of the contrast is therefore easily evaluated in terms of the coefficients (7)

---

[1] As shown in [24] the original master equation by Gallis and Fleming [25] predicts a localization rate that is too large by a factor of 2π. It would yield an additional 2π in the exponent of (7). The experimental results discussed in Sect. 4 are sensitive to this factor (and rule it out).

and (4). Using $p = n k_B T$ gives

$$
V_\lambda(p) = \frac{2|B_2^{(\lambda)}| \left(B_1^{(0)}\right)^2}{\left(B_0^{(0)}\right)^3} \exp\left(-\frac{2L\sigma_{\mathrm{eff}}}{k_B T} p\right)
$$

$$
= V_\lambda(0) \exp(-p/p_0) . \qquad (10)
$$

Hence, an exponential decrease of the visibility as a function of the gas pressure p is expected. This is the expected experimental signature of collisional decoherence. It should not be confused with Beer's law for absorption which predicts an exponential decrease of the mean signal at constant visibility.

## 4   Experimental decoherence: the pressurized interferometer

A first experimental indication of collisional localization is presented in Fig. 3. It shows the change in the interference pattern of C_{70} if a small amount of argon gas is added to the vacuum chamber. A significant reduction in visibility is observed from 42% to 34% if the pressure in the chamber is increased from 3×10^{-8} mbar to 5×10^{-7} mbar. The horizontal shift between the two curves is not significant since it can be explained by thermal drifts of the setup between the two recordings. In contrast to that, the values of the visibilities are significant. It was tested that they were reproducible within ± 2 percent on different days over several weeks.

The visibility is then recorded for a series of interferograms at different gas pressures. A typical result is given in Fig. 4, which shows the pressure dependence of the interference visibility in the presence of thermal argon gas. As expected from (10) an exponential decay is observed. Given the high initial contrast this is clear evidence for the occurrence of collisional decoherence.

The good quantitative agreement with decoherence theory is obtained after taking into account a modification that is related to the particular method of velocity selection used in the
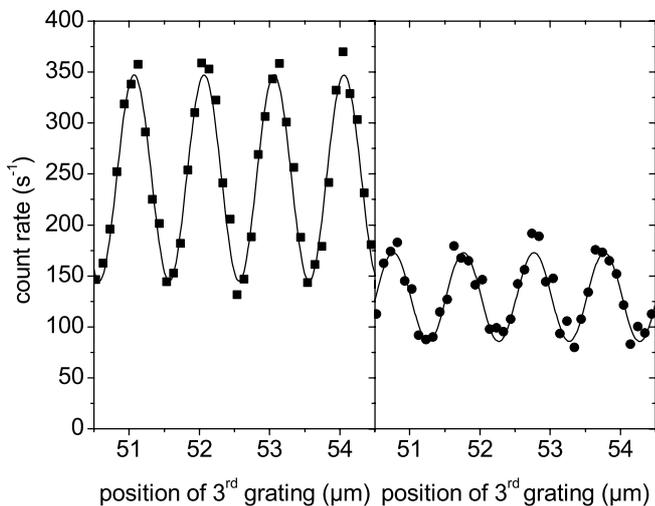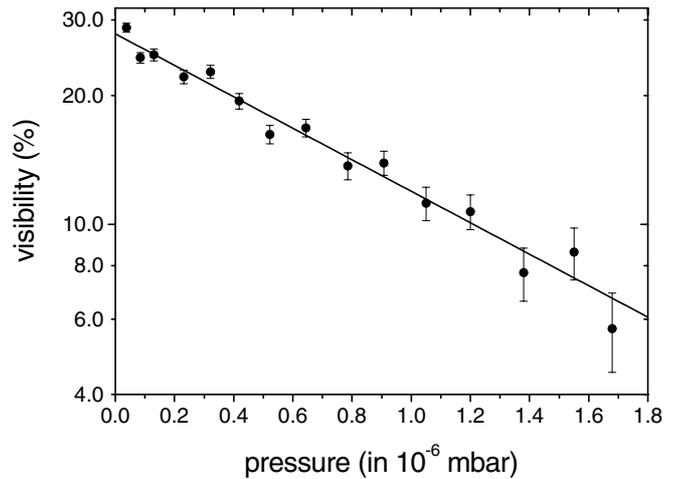
FIGURE 4   Visibility of the C_{70} fringes as a function of the argon pressure at room temperature. The experimental data are given by *full circles* and the theoretical prediction (10) gives the slope of the *solid line*. The data follow very nicely the expected exponential decay proving the occurrence of collisional decoherence. This experiment was done with $L = 22$ cm

experiment. As discussed in Sect. 2 a gravitational velocity selection scheme is employed by restricting the molecular beam to a free-flight parabola. If the apparatus is filled with a gas this velocity selection gets disturbed by collisions outside of the interferometer. After a collision each molecule gets slightly deflected so that now fullerenes with a 'wrong' velocity may fit through the setup. At the same time the molecule detector has only a finite size so that some of the molecules will pass it undetected after a collision. One has to take into account the small modification of the expected decay of visibility due to these effects. This is done by solving the classical phase space dynamics, i.e., the Boltzmann equation, effectively by a Monte Carlo method. The scattering angles are determined from the (diffraction limited) differential cross sections. Semiclassical expressions for the latter can be found in [27].

The predictions for the visibility are obtained by weighting (10) with the classical velocity distribution in the detector – which corresponds to an averaging over a distribution of de Broglie wavelengths. Also the reduction of the mean count rate found in Fig. 2 is well reproduced by the calculation.

The loss of coherence with increasing pressure is conveniently described by the 'decoherence pressure' p_0 defined in (10). Table 1 compares the measured values of p_0 to the theoretical predictions for a number of gases. One observes satisfactory agreement over the whole mass range which covers two orders of magnitude. The experimental error is mainly due to the uncertainty in the pressure measurement, which is about 15%.

The most remarkable feature of the results reported in Table 1 is the very weak dependence of the decoherence pressure on the type of gas used. This can be explained by assuming that the polarizability of the gas particle is proportional to its mass m_g. Then also C_6 is proportional to m_g, and one observes from (9) that the mass dependencies of the interaction constant and of the most probable gas velocity $\tilde{v}_g$ almost cancel out leaving $\sigma_{\mathrm{eff}} \sim m_g^{1/10}$. The observed variations in Table 1 are due to deviations from the assumed proportion-

FIGURE 3   *Left*: C_{70} interference fringes at a pressure of 3×10^{-8} mbar (residual background gases) shown as *full circles*. *Right*: the same signal in the presence of argon gas, at a pressure of 5×10^{-7} mbar. The *lines* are fits of a sine function. The mean velocity of the fullerene molecules was 189 m/s

Atom	H_2	D_2	He	CH_4	Ne	N_2	Air	Ar	CO_2	Kr	Xe	SF_6
mass/amu	2	4	4	16	20.2	28	28.8	39.9	44	83.8	131.3	146
p_0 (theo.)	7.3	9.2	13.8	7.9	16.0	11.3	11.3	11.8	N.A.	12.4	11.5	N.A.
p_0 (exp.)	4.6	8.0	10.7	8.1	13.2	11.5	10.5	10.8	8.9	12.9	10.6	11.3
Δp_0 (exp.)	0.7	1.2	1.6	1.2	2.0	1.7	1.6	1.6	1.3	1.9	1.6	1.7

TABLE 1   Decoherence pressures, i.e. pressures for $V_\lambda(p)/V_\lambda(0) = e^{-1}$ for various collision gases as found in the short interferometer with $L = 22$ cm, at a mean molecular speed of $v_m = 117$ m/s. Note the very weak dependence on the mass of the colliding partner. All pressures given in units of 10^{-7} mbar

ality and reflect the specific electronic structures of the gas particle.

It should be noted that the best contrast for all experiments contributing to Table 1 was systematically smaller than that of Fig. 2. Although the whole experiment was mounted on top of an optical table with active pneumatic vibration isolation it was possible to identify tiny vibrations of the interferometer, induced by the water flow in the laser cooling system, as being the cause of a reduced contrast. The visibility was increased by about 10% when the laser was set on rubber feet. This simple remedy was applied for the experiments in the extended interferometer ($L = 38$ cm) of Figs. 1, 2, 3, 5 but not yet for the experiments of Fig. 4 and Table 1 ($L = 22$ cm).

However, it is important to note that the influence of external vibrations and the effect of collisional decoherence are independent of each other, and their total effect can therefore be obtained by multiplying their respective contributions to the reduction in visibility. This assumption was experimentally verified for several gases: a varying initial (low-pressure) contrast always led to the same slope in the visibility-vs-pressure curve, i.e., to the same decoherence pressure. The validity of Table 1 is therefore not compromised by potential mechanical perturbations.

However, the total time of flight plays an important role for the absolute value of the fringe contrast. Clearly, for slow molecules the interaction time with the gratings is longer, and vibrations will be more detrimental. Also, the effective cross section (9) increases for decreasing molecular velocities. In Fig. 5 the increasing influence of collisions is observed in an interferometer filled with argon, for various fullerene velocities, i.e. various interaction times. In contrast to the experiment of Fig. 2, the central height delimiter was set to 150 μm (instead of 50 μm). This increased the flux but it also reduced the overall contrast by a few percent, both due to the increased sensitivity to imperfections in the grating alignment and due to an increased width of the velocity distribution.

Figure 5 shows the experimental visibility curves for $p_{low} = 3 \times 10^{-8}$ mbar (full circles) and $p_{high} = 5 \times 10^{-7}$ mbar (hollow circles) and compares them to the quantum calculation (solid and dashed line, respectively) with the same model parameters as already used for Fig. 2. The remarks of the discussion of Fig. 2 apply also here. This holds for the reduction of the visibility at long wavelengths due to vibrations, the shift of the maxima with respect to the Talbot length and the asymmetric line shapes, caused by the molecule-wall interaction. The new feature in this graph is the contrast reduction due to the scattering events in the Argon atmosphere and their dependence on the interaction time. For wavelengths in the 2.5 pm regime ($v \sim 200$ m/s) the pres-
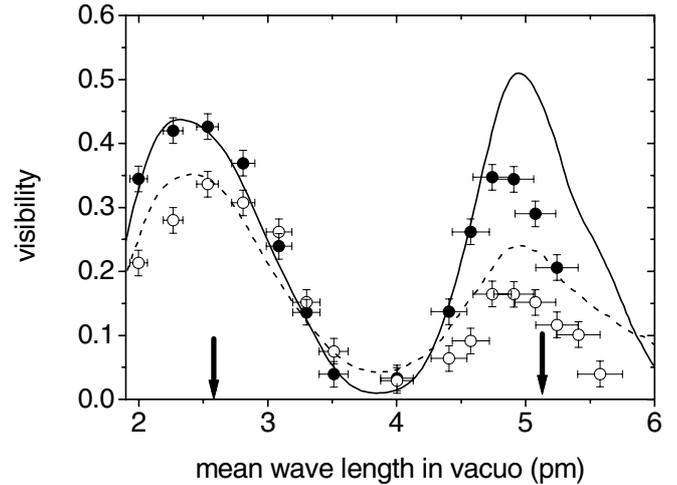
FIGURE 5   Pressure dependence of the visibility in the stretched Talbot Lau interferometer (height delimiter at 150 μm). The main feature in this plot is the strong dependence of the interference visibility on the molecular wavelength, i.e. the molecular velocity. As expected, the slow molecules are much stronger affected by collisions than the fast ones. The experimental and theoretical curve for a background pressure of $p = 3 \times 10^{-8}$ mbar are given by the *full circles* and a *solid line*. The *hollow circles* and the *dashed line* represent the data for argon at $p = 5 \times 10^{-7}$ mbar. The overall good agreement between theory and experiment deteriorates markedly in the regime of long wavelengths, i.e. small velocities, where residual vibrations of the interferometer are expected to be relevant

sure increase leads to $V_\lambda(p_{high})/V_\lambda(p_{low}) = 0.8$ whereas for wavelengths in the 5 pm regime ($v \sim 100$ m/s) the increased pressure results in $V_\lambda(p_{high})/V_\lambda(p_{low}) = 0.5$. These ratios are identical for theory and experiment, both for the slow and for the fast molecules. However, the absolute values still differ at long wavelengths. Again this shows that the different decoherence mechanisms (collisions and vibrations) are independent of each other and their effects can be considered as separate multiplicative factors to the visibility.

5   Conclusion

The experiments have demonstrated the periodic nature of the Talbot–Lau effect in a molecule interferometer by observing a visibility recurrence in the elongated setup ($L = 38$ cm). The increased grating separation permitted a detailed quantitative study of decoherence due to collisions with the background gas. The experiments show that decoherence by scattering of small particles, which is ubiquitous in our macroscopic world, can be understood and well controlled under high vacuum conditions. Based on the good agreement which was found in comparing the experiments with the numerical simulations it is now possible to estimate the residual

object	C_{70}	insulin	GFP[a]	hemoglobin	ferritin	virus[b]
mass (amu)	840	5730	2.7×10^4	6.4×10^4	4.8×10^5	8×10^6
min/max extension (nm)	1	3	3/4	5/7	10	30
estim. σ_{eff} (nm^2)	730	1900	3700	5200	1.1×10^4	3.6×10^4
estim. p_0 (mbar)	3×10^{-8}	1×10^{-8}	6×10^{-9}	4×10^{-9}	2×10^{-9}	6×10^{-10}

[a] green fluorescent protein
[b] rhinovirus HRV2 S150

TABLE 2   Estimated decoherence pressures of candidates for matter wave interferometry in a stretched Talbot interferometer ($L = 1$ m, $v_m = 10$ m/s) in the presence of air. The effective cross sections are based on reasonable estimates for the polarizability and the effective number of valence electrons

gas pressures required to observe the quantum nature of much larger objects.

To be specific, consider a set of proteins of increasing size up to the mass of a rhinovirus, interacting with molecular nitrogen (300 K, polarizability $\alpha/\text{Å}^3 = 4\pi\varepsilon_0 \times 1.75$). Since the static polarizability of large hydrocarbons is closely proportional to their mass M, i.e., $\alpha/\text{Å}^3 = 4\pi\varepsilon_0 \times 0.123\, M/\text{amu}$, it is possible to use the Slater–Kirkwood approximation [28].

For the observation of interference with supermassive molecules one needs low velocities in order to get de Broglie wavelengths larger than 100 fm. For particles in the mass range of 10^5 amu this requires velocities of the order of $v_m = 10$ m/s. Although this is a rather demanding requirement it seems not impossible to develop appropriate sources in the future. Moreover, a realistic earth-bound interferometer would be limited to a Talbot length of $L \sim 1$ m.

Based on these assumptions Table 2 extrapolates the decoherence pressures for insulin, green fluorescent protein, hemoglobin, ferritin, and a human rhinovirus. It turns out that the vacuum conditions for quantum interference of these objects can be provided using commercially available technology.

REFERENCES

1 P.R. Berman (Ed.): *Atom Interferometry* (Acad. Press, New York 1997)

2 M. Arndt, O. Nairz, J. Voss-Andreae, C. Keller, G.V. der Zouw, A. Zeilinger: Nature **401**, 680 (1999)

3 M. Arndt, O. Nairz, A. Zeilinger: In *Quantum [Un]Speakables*, ed. by R. Bertlmann, A. Zeilinger (Springer, Berlin 2002) pp. 333–351

4 E. Joos, H.D. Zeh: Z. Phys. B. **59**, 223 (1985)

5 W.H. Zurek: Phys. Today **44**(10), 36 (1991)

6 M.S. Chapman, C.R. Ekstrom, T.D. Hammond, R.A. Rubenstein, J. Schmiedmayer, S. Wehinger, D.E. Pritchard: Phys. Rev. Lett. **74**, 4783 (1995)

7 K. Hornberger, S. Uttenthaler, B. Brezger, L. Hackermüller, M. Arndt, A. Zeilinger: Phys. Rev. Lett. **90**, 160401 (2003)

8 C.J. Myatt, B.E. King, Q.A. Turchette, C.A. Sackett, D. Kielpinski, W.M. Itano, C. Monroe, D.J. Wineland: Nature **403**, 269 (2000)

9 S. Reynaud, B. Lamine, A. Lambrecht, P.M. Neto, M.-T. Jaekel: Int. J. Mod. Phys. A **17**, 1003 (2002)

10 O. Nairz, M. Arndt, A. Zeilinger: J. Mod. Opt. **47**, 2811 (2000)

11 W. Schöllkopf, J.P. Toennies: Science **266**, 1345 (1994)

12 C. Bordé, N. Courtier, F.D. Burck, A. Goncharov, M. Gorlicki: Phys. Lett. A **188**, 187 (1994)

13 C. Lisdat, M. Frank, H. Knöckel, M.-L. Almazor, E. Tiemann: Eur. Phys. J. D **12**, 235 (2000)

14 R. Brühl, P. Fouquet, R.E. Grisenti, J.P. Toennies, G.C. Hegerfeldt, T. Köhler, M. Stoll, C. Walter: Europhys. Lett. **59**, 357 (2002)

15 J. Clauser, M. Reinsch: Appl. Phys. B **54**, 380 (1992)

16 K. Patorski: In *Progress in Optics XXVII*, ed. by E. Wolf (Elsevier Science Publishers B.V., Amsterdam 1989) pp. 2–108

17 M.S. Chapman, C.R. Ekstrom,, T.D. Hammond, J. Schmiedmayer, B.E. Tannian, S. Wehinger, D.E. Pritchard: Phys. Rev. A **51**, R14 (1995)

18 L. Deng, E.W. Hagley, J. Wen, M. Trippenbach, Y. Band, P.S. Julienne, J.E. Simsarian, K. Helmerson, S.L. Rolston, W.D. Phillips: Nature **398**, 218 (1999)

19 J.F. Clauser, S. Li: Phys. Rev. A **49**, R2213 (1994)

20 B. Brezger, L. Hackermüller, S. Uttenthaler, J. Petschinka, M. Arndt, A. Zeilinger: Phys. Rev. Lett. **88**, 100404 (2002)

21 B. Brezger, M. Arndt, A. Zeilinger: J. Opt. B **5**, S82 (2002)

22 K. Hornberger et al.: in preparation

23 H.B.G. Casimir, D. Polder: Phys. Rev. **73**, 360 (1948).

24 K. Hornberger, J.E. Sipe: Phys. Rev. A **68**, 012105 (2003)

25 M.R. Gallis, G.N. Fleming: Phys. Rev. A **42**, 38 (1990)

26 G.C. Maitland, M. Rigby, E.B. Smith, W.A. Wakeham: *Intermolecular Forces – Their Origin and Determination* (Clarenden Press, Oxford 1981)

27 R. Helbing, H. Pauly: Z. Phys. **179**(0), 16 (1964)

28 R.B. Bernstein: *Atom-Molecule Collision Theory* (Plenum, New York 1979)